Acoustic Transmission Loss in Hilbert Fractal Metamaterials

Gianni Comandini[1,2,*], Morvan Ouisse[2], Valeska P. Ting[1,3], and Fabrizio Scarpa[1]

[1]Bristol Composite Institute (BCI), School of Civil, Aerospace and Mechanical Engineering (CAME), University of Bristol, Bristol, United Kingdom
[2]SUPMICROTECH, Université de Franche-Comté, CNRS, Institut FEMTO-ST, 25000-FR Besançon, France
[3]Research School of Chemistry, Australian National University, Canberra, ACT 2601, Australia
[*]gianni.comandini@bristol.ac.uk

ABSTRACT

Acoustic metamaterials are increasingly being considered as a viable technology for sound insulation. Fractal patterns constitute a potentially groundbreaking architecture for acoustic metamaterials. We describe in this work the behaviour of the transmission loss of Hilbert fractal metamaterials used for sound control purposes. The transmission loss of 3D printed metamaterials with Hilbert fractal patterns related to configurations from the zeroth to the fourth order is investigated here using impedance tube tests and Finite Element models. We evaluate, in particular, the impact of the equivalent porosity and the relative size of the cavity of the fractal pattern versus the overall dimensions of the metamaterial unit. We also provide an analytical formulation that relates the acoustic cavity resonances in the fractal patterns and the frequencies associated with the maxima of the transmission losses, providing opportunities to tune the sound insulation properties through control of the fractal architecture.

Introduction

Excessive noise can significantly impact human health and lead to serious pathology[1,2]. Traditional noise transmission mitigation strategies[3,4] have followed mass law principles[5], with a resulting drawback in terms of high mass and thickness of the materials used[6]. Mass-spring-mass models exploit other mechanisms, with the development of designs based on one or multiple coupled degrees of freedom and combinations of materials[7]. Spring-mass models are typically used in acoustic architecture to separate environments with rational use of the space available. Other more recent but consolidated technologies exploit the use of porous materials as perforated[8–10] and/or microperforated panels[11], or through thermo-viscous acoustic energy dissipation in the internal porous skeletons of foams with various internal geometry and materials compositions[12–16]. Thermo-viscous energy dissipation technologies also theoretically allow acoustic dampening of any frequency, with the only limitation represented by the available room for the porous liners. Because of space constraint limitations, porous materials are generally adopted to mitigate noise within the middle and high-frequency ranges. Another technique to obtain a desired transmission loss (TL) for a predetermined interval of frequencies is by using Helmholtz resonators[17–20]. However, resonators are only efficient for narrow sets of frequency ranges and may involve the use of considerable space for the spring part of the Helmholtz resonator for low frequencies applications[21,22]. More recent techniques for noise management are promising because of their lightweight characteristics and their use of different mechanisms to achieve sound absorption and transmission loss[16,23–30]. Metamaterials for noise control are moving from conceptual design[31–34] to practical implementation[35–42]. Fractal geometries have been used to design electromagnetic and mechanical metamaterials[43–46]. Moreover, fractal mechanical metamaterials possess strength, shape stability under large deformations, and significant damage tolerance[47]. The Hilbert lattice[48] is one of the most heavily explored fractals in metamaterial design, especially for electronics/electromagnetic applications. Fractal antennas have shown enhanced performance compared to traditional designs since they can operate at multiple frequencies without load and are more compact than those featuring other geometries[49–52]. Recent studies in the field of acoustics have improved the understanding of the Hilbert space-filling curve pattern in metamaterials, providing numerous benefits ranging from high porosity, multiple resonances, multi-modes, and sub-wavelength scales[53,54]. This work describes, for the first time, a numerical and experimental evaluation of the acoustic transmission loss capability of Hilbert fractal metamaterials.

A point of particular novelty here is in the improved understanding of the physics behind the frequencies corresponding to transmission loss peaks. As will be demonstrated, those frequencies correspond to the phenomenon of impedance mismatch, with an analytical formulation that describes how to calculate those frequencies also being presented. Furthermore, we demonstrate that the use of the Hilbert fractal pattern to design passive tools for acoustic control relies on the capability of the metamaterials geometries to provide tunable transmission loss in the lower part of the acoustic spectrum. This is an advantage

when compared with commonly used acoustic porous materials having the same thickness[55,56] or - more significantly - to the narrow-band effect of Helmholtz resonators[57,58] or straight slits with similar or narrower widths (see the Supplementary Information).

The fractal topologies covered here range from the 0^{th} (Fig.1*a*) to the 4^{th} order (Fig.1*e*). We have used additive manufacturing to generate samples of fractal metamaterials made using polylactic acid (PLA) because of its recyclability and good printability. One of the design features of the fractal specimens is the presence of inlets and outlets for the impinging and exiting acoustic waves (Fig.1$a-e$). The geometry of the fractal patterns is here defined in nondimensional terms, using the lateral dimension of the metamaterial sample n (50.8 *mm* in our case), the gap width w (see Fig.1g), and the fractal order ξ. The parameter $\eta = w/n$ represents the ratio between gap width (w) and side dimension of the specimen (n); meanwhile, the porosity is defined as $\varphi = \eta(2^{\xi})$.

An impedance tube with four microphones was used to obtain the experimental measurements of the TL (Fig.1*i*). Numerical Finite Element simulations using COMSOL Multiphysics[59] featuring different models representing the air inside the cavities of the fractal metamaterials, and analytical models were also performed. The models were used here to benchmark the results and understand some of the physical mechanisms underpinning the amplitude and frequency of the TL peaks.

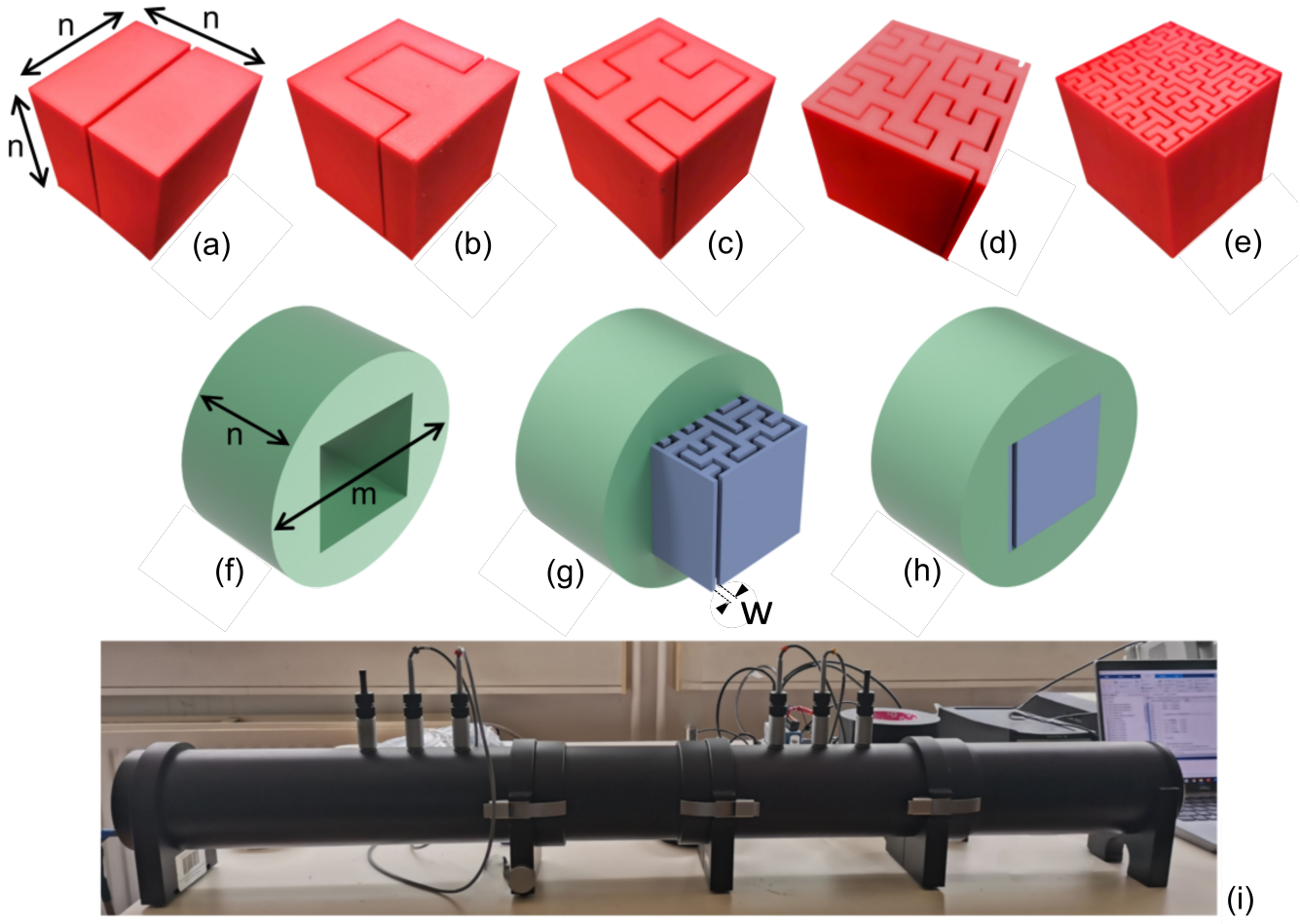

Figure 1. The Hilbert fractal acoustic metamaterials and the impedance tube used in this work. (a) The 0^{th} order with underlined n, the side dimension of the cube - 50.8 *mm*, in this case. (b) 1^{st}, (c) 2^{nd}, (d) 3^{rd}, and (e) 4^{th} orders of the Hilbert fractal. (f) Sample holder used for the samples inside the test room of the impedance tube. The holder has an external diameter m of 100 *mm* and thickness n of 50.8 *mm*. (g) Example of the cubic specimen (d), having been partially inserted into the holder (f), showing the gap width w. (h) Holder and sample completely assembled. (i) The impedance tube.

Results and Discussion

We performed a comparison between experimental and finite element-simulated transmission losses for the Hilbert fractal metamaterials with a gap width of 1.0 *mm* (i.e., corresponding to a value of η equal to 2 %). The size of the gap is the same

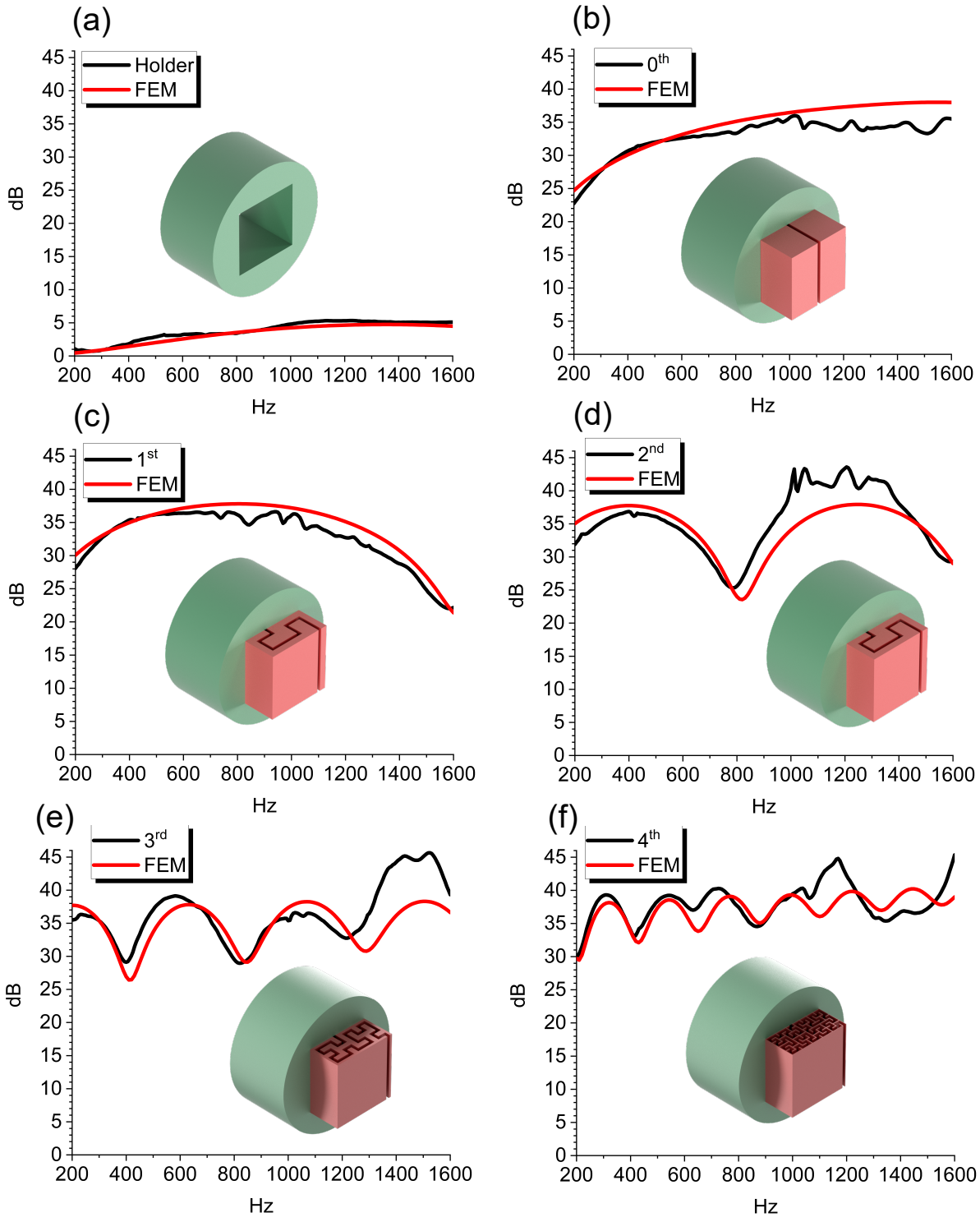

Figure 2. Comparison of the transmission loss between experimental results (black) and FEM (red) for the various Hilbert fractal orders. All the measurements and simulations were made taking into account the cylindrical holder of Fig.1*f*. (a) Only the holder (Fig.1*f*). (b) Zeroth (Fig.1*a*). (c) First (Fig.1*b*). (d) Second (Fig.1*c*). (e) Third (Fig.1*d*). (f) Fourth (Fig.1*e*) orders.

on both sides of the sample. The finite element results here are related to narrow-acoustics models of the cavity[59] inside the fractal metamaterials. There is a good agreement between experiments and simulations, as can be seen in Fig.2. As also shown in the Supplementary Information (Fig.S2), Hilbert geometries from the second order with $w = 1\,mm$ can provide a greater transmission loss compared to a block of bulk PLA with the same dimension n. The mechanism that generates the peaks of the transmission loss is an impedance mismatch between the air inside the tube and the metamaterial.
The metamaterial provides an increasing number of minimum transmission coefficient (TC) values in the frequency spectrum investigated according to the fractal order, whereas the peaks of the transmission loss correspond to frequencies related to the minimum TC values. The transmission loss has a behaviour similar to an inverse pass filter, for which the transmission loss is maximum and therefore the TC is at its minimum. Moreover, as shown in Fig.S4, the high values of the peak of the reflection coefficient highlight the multi-resonance behaviour due to the Fabry–Pérot resonance. The sample made of bulk PLA has its own Fabry–Pérot resonant frequencies. Those however lie outside the spectrum of frequencies investigated in this work.

At the same time, the metamaterial can minimise and maximise the mismatch at multiple frequencies, as shown in Fig.S4. A dip in the reflection coefficient corresponds to a drop in the transmission loss output. The fractal acoustic metamaterial can therefore provide multiple maximisations and minimisations of the impedance mismatch by a single fractal geometry cavity. A description of the model, and a comparison between lossless, viscous and experimental results related to configurations from the 0^{th} to the 4^{th} fractal order are presented in the Supplementary Information. Both viscous-based and lossless formulations for the fluid are able to capture the overall transmission loss properties inside the fractal cavities, and the narrow-acoustics simplification is adequate to follow the experimental results; moreover, as described by the work of *Ward, et al*[60], the particle velocity field inside the fractal channels is lower when thermoviscous losses are considered in the FEM model, as shown in the Supplementary Information Fig.S5. The lossless model however provides large dips of transmission loss at frequencies slightly larger than those predicted by the viscous models, and provided by the experimental results. It is interesting to note the behaviour of the TL for the various configurations. The order zero (i.e., the topology with the cavity extending to the full length of the cubic sample - Fig.1*a*). has a peak of the transmission loss equal to 37 dB at 1546 Hz (Fig.2*b*). A peak of 37 dB is however observed at 785 Hz in the case of the first fractal order (Fig.2*c*). The second Hilbert fractal order possesses two peaks at 390 Hz and 1212 Hz, both with TL values of 37 dB and 38 dB, respectively (Fig.2*d*). The third order shows the presence of four transmission loss peaks at 195 Hz, 611 Hz, 1033 Hz, and 1455 Hz, all with a TL value of 38 dB (Fig.2*e*). Finally, the fourth fractal order exhibits seven TL peaks at 310 Hz, 526 Hz, 743 Hz, 961 Hz, 1180 Hz, 1399 Hz, and 1618 Hz, with TL values of 38 dB, 38 dB, 39 dB, 39 dB, 40 dB, 40 dB, and 41 dB, respectively (Fig.2*f*). We also include the results related to the transmission losses of the empty holder (Fig.1*f*); as expected, the TL values here were the lowest amongst all the configurations considered (Fig.2*a*). In summary, both experiments and simulations show the presence of multiple peaks and minima of the transmission loss; the number of those peaks and dips depends on the fractal order of the pattern of the metamaterial considered. The maxima of the transmission loss all show a nearly constant magnitude, with their position dependent on the length of the fractal and, consequently, on a higher Hausdorff dimension[61]. Despite the complexity of the acoustic behaviour of these fractal-shaped metamaterials, it is possible to identify some general trends in their TL response. Increased fractal orders feature larger numbers of TL peaks with a very similar magnitude (see Table 2 and Fig.3*c*)). This behaviour can be explained by observing that the performance of the TL magnitude of the metamaterial is mainly dependent upon the geometry of the opening slot, rather than on the fractal order itself.

Gap Width η	Fractal Order ξ	Porosity φ	TL [dB]
2%	0^{th}, 1^{st}, 2^{nd}, 3^{rd}, 4^{th}	2%, 4%, 8%, 16%, 31%	37
4%	0^{th}, 1^{st}, 2^{nd}, 3^{rd}, 4^{th}	4%, 8%, 16%, 31%, 63%	31
6%	0^{th}, 1^{st}, 2^{nd}, 3^{rd}, 4^{th}	6%, 12%, 24%, 47%, 94%	27
8%	0^{th}, 1^{st}, 2^{nd}, 3^{rd}	8%, 16%, 31%, 63%	25
10%	0^{th}, 1^{st}, 2^{nd}, 3^{rd}	10%, 20%, 39%, 79%	23
12%	0^{th}, 1^{st}, 2^{nd}, 3^{rd}	12%, 24%, 47%, 94%	21
14%	0^{th}, 1^{st}, 2^{nd}	14%, 28%, 55%	19
16%	0^{th}, 1^{st}, 2^{nd}	16%, 31%, 63%	18
18%	0^{th}, 1^{st}, 2^{nd}	18%, 35%, 71%	17
20%	0^{th}, 1^{st}, 2^{nd}	20%, 39%, 79%	16

Table 1. Normalized gap, fractal orders, porosity, and TL values for the classes of fractal metamaterials evaluated in this work. The leftmost column shows the normalized gap values, while the second column displays the corresponding fractal orders, which are proportional to the gap width. The third column contains the equivalent porosity of each fractal order in terms of relative gap width. The fourth column shows the values of the peaks of the transmission loss calculated via FEM and related to the first cavity mode of the fractals for a given gap width.

Fractal Order ξ	Mode Number	FEM Mean [Hz]	Normalised Standard Deviation	Eq. 1
0^{th}	1^{st}	1472.2	1.6%	1548.7
1^{st}	1^{st}	811.2	0.3%	807.3
2^{nd}	1^{st}	426.6	0.8%	412.6
2^{nd}	2^{nd}	1295.3	1.3%	1237.7
3^{rd}	1^{st}	224.8	0.8%	208.6
3^{rd}	2^{nd}	685.3	1.1%	625.8
3^{rd}	3^{rd}	1148	1.5%	1043
3^{rd}	4^{th}	1602.5	1.3%	1460.2
4^{th}	1^{st}	328	0.8%	314.7
4^{th}	2^{nd}	553.7	0.7%	524.5
4^{th}	3^{rd}	781	1.1%	734.3
4^{th}	4^{th}	1008	1.1%	944.1
4^{th}	5^{th}	1235.3	1.0%	1153.9
4^{th}	6^{th}	1462.7	1.2%	1363.7
4^{th}	7^{th}	1689.3	1.3%	1573.5

Table 2. Cavity resonances predicted via Finite Element (narrow viscous model) and the analytical formulation for the various fractal orders. The Finite Element results related to each mode are calculated by averaging the values of those modes over the different gap widths considered in this work. The standard deviations of those frequencies are normalised against the corresponding average value. The last column refers to the analytical resonance frequency related to an open-closed cavity.

Table 1 shows the dependence of the magnitude of the transmission loss peak values from the FEM simulations versus the normalised gap width, the fractal orders and the porosity of the metamaterials. One can notice that the most significant factor affecting the values of the transmission losses is the gap width, regardless of the fractal order or porosity considered (see also Fig.3*c*). Of particular interest is also the effect of the fractal orders on the frequencies corresponding to the peak of the transmission losses, which are also known to affect the acoustic absorption properties of Hilbert fractal metamaterials[53]. The results suggest that while the order of the fractal pattern can impact both peak TL magnitudes and related frequencies, it is not the dominant factor to control those frequencies in configurations with varying normalised gap widths. Furthermore, the results indicate that variations of the porosity have a limited effect on the transmission losses (Fig.3*c* and Table 1).

The results from the experimental and numerical transmission losses show that the frequencies corresponding to the peak of the TL can be approximated using equation (Eq.1), which is also adopted for the design of musical (wind) instruments[62,63]. Formula (Eq. 1) is related to open-closed one-dimensional resonating cavities and considers even harmonics only (i.e., $r = m+1$ with $m \in \mathbb{N}$)[62]. The resonant frequency for an open-closed cavity representing the fractal path is equal to:

$$f_n = \frac{rc}{4(L+\Delta L)} \tag{1}$$

In Eq. 1, c is the speed of sound in air, 343 m/s and $L = n(2^{\xi})$ is the length of the fractal cavity inside the metamaterial sample, and ΔL is the extra length of the fractal channel that needs to be considered due to thermoviscous losses[60,64]. The term ΔL is equal to $\frac{8w}{3\pi}$ [60]. A comparison of the normalised standard deviations of the of the frequencies related to peaks of the TL and calculated via FEM and the analytical formulas is shown in Fig.S6 of the Supplementary Information. The analytical formulas include the terms $\Delta L = 0$ (Fabry–Pérot model) and $\Delta L = \frac{8}{3\pi^{\frac{3}{2}}}\sqrt{nw}$[64].

At the frequencies corresponding to the various cavity modes of the fractal patterns, the peak of the TL is always close to a value of 37 dB; this is true also within the low-frequency range within 250Hz - 400Hz if the percentage opening on both sides of the metamaterial is 2%, no matter the fractal order considered (Table 1). This simplification is valid, especially for the case of the first peaks related to the first acoustic modes in the lower frequency range (Table 1). Table 2 summarises the numerical (narrow-acoustic approximation[59]) and analytical results related to the TL for different gap widths and fractal orders. The vibrational modes corresponding to the TL peaks are also indicated. The standard deviation of the distribution of frequencies associated with transmission loss peaks for the different gap widths is normalised against the value of 1688 Hz, which corresponds to the average frequency of the TL peak related to the 0^{th} order when the gap width (η) is varied from 2% to 20% (Fig.3d-g). Notably, the frequency corresponding to the TL peaks predicted by the analytical open-closed resonator formula is also close to the numerical FE one (Table 2, fifth column). The number of vibrational modes within the frequency range investigated here increases with the increasing fractal order, and the frequencies related to the TL peaks shift to higher

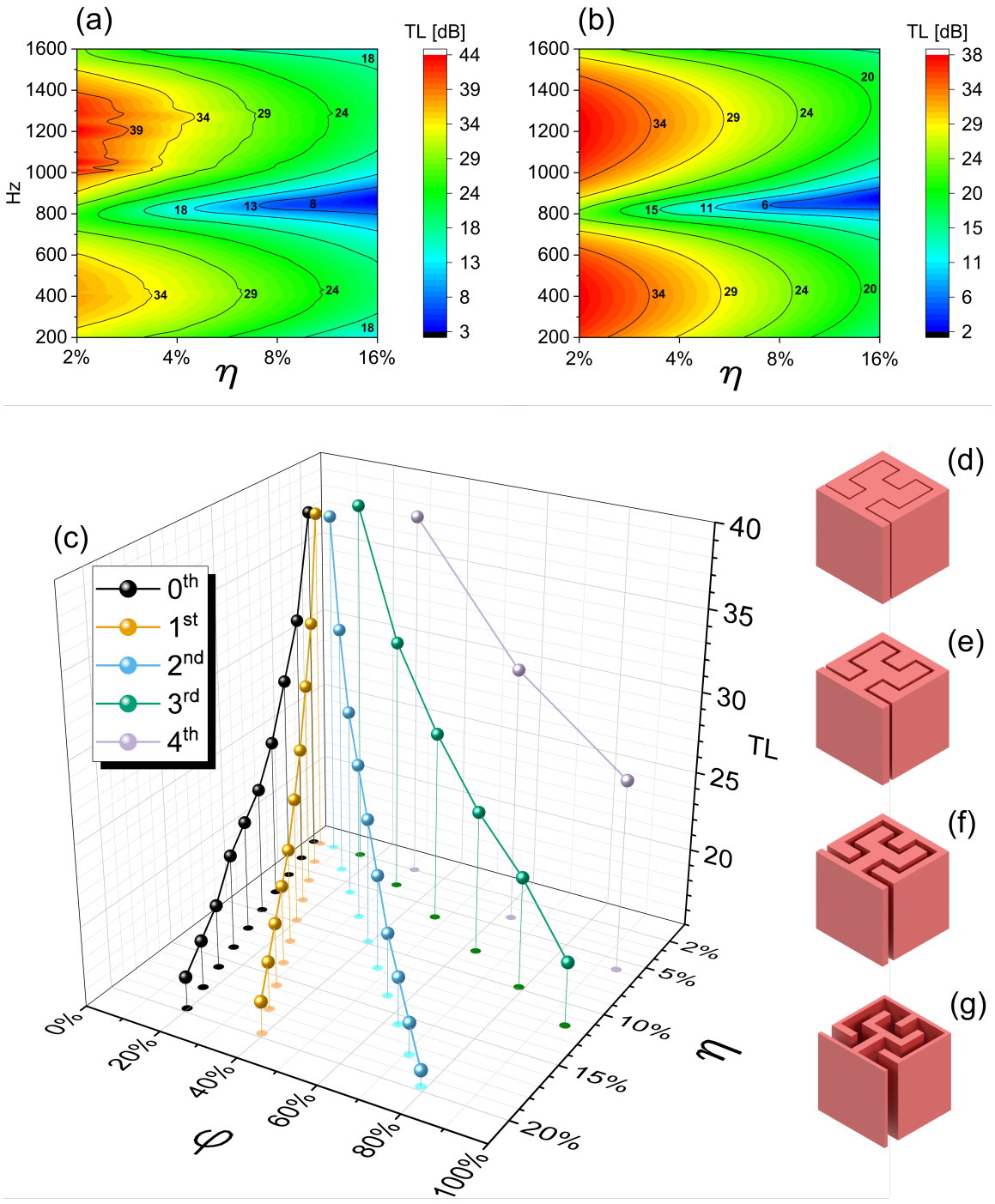

Figure 3. Experimental (a) and FE (b) contour plots of the TL as a function of the frequencies and normalised gap widths. (c) Variation of the transmission loss peaks calculated via FEM for the fractal orders and their porosity when the normalised gap changes. Example of the 2^{nd} order Hilbert fractal with a gap width of (d) 1 *mm*, (e) 2 *mm*, (f) 4 *mm*, and (g) 8 *mm*.

values. The magnitudes of TL peaks are again almost constant, with only slight variations attributed to the change in the length of the fractal pattern inside the metamaterial. These findings imply that by increasing the fractal order, it is possible to achieve more resonant peaks, resulting in more effective broadband transmission loss, and also sound absorption[53]. Moreover, both numerical and analytical modelling approaches provide a good approximation of the actual behaviour of these fractal acoustic metamaterials (Fig.2, and Fig.3$a-b$).

Conclusion

This work has shown the relationship between the fractal order and the transmission loss in acoustic metamaterials with Hilbert fractal patterns. The equivalent porosity and gap widths play a crucial role in determining the values of the transmission loss (Fig. 3c), with the gap width being the most significant factor impacting the magnitudes of the TL (Fig.3$a-b$ and Table 1) that create the impedance mismatch responsible for the generation of the TL maxima. Our experimental and numerical results show that a decrease in the transmission loss is generated by the increase of the gap width, with a consequent reduction of the performance of the acoustic metamaterial. We have also investigated the influence of fractal order on transmission loss. Our simulations show that the fractal order plays a role in determining the number of TL peaks, but not in their magnitude. Finally, the frequencies corresponding to the peaks of the transmission losses can be well approximated and predicted by considering the fractal patterns as open-closed one-dimensional cavities and calculating the corresponding resonance frequencies. The formula 1 makes it possible at the design stage to relate those frequencies to the fractal order and nondimensional gap width of the fractal acoustic metamaterial.

Methods

All the samples were printed using the Raise3D Pro3 Plus 3D Printer. The machine was set up with a 0.1 *mm* layer height, 100% infill density, and an extrusion nozzle of 0.4 *mm*. 3DJake recycled PLA was used as the filament. The transmission loss have been measured following the ASTM E2611-09 standard[65], using a Brüel & Kjær impedance tube (Fig.1i) with a four microphones configuration and double load measurements. The gap widths of the metamaterials samples are 1 *mm*, 2 *mm*, 4 *mm* and 8 *mm*, corresponding to 2% (Fig.3d), 4% (Fig.3e), 8% (Fig.3f) and 16% (Fig.3g). All the tests were performed by mounting the fractal metamaterial sample in a cylindrical holder (Fig.1$f-h$). The FEM simulations were performed using the Comsol Multiphysics 5.6 software[59] with a 3D model of the impedance tube and the metamaterials specimens[53]. The FEM model does not consider the presence of the PLA material, only the fluid cavity is modelled, with loss-less, thermoviscous and narrow-viscous domains. The part of the impedance tube model outside the test room was represented with a lossless air fluid, with probes simulating the position of the four microphones. The frequency range investigated in both FEM and experiments was from 200 Hz to 1600 Hz.

Acknowledgements

G.C. acknowledges the support of UK EPSRC through the EPSRC Centre for Doctoral Training in Advanced Composites for Innovation and Science [EP/L016028/1], and Rafael Heeb, Emanuele De Bono and Martin Gillet for technical assistance. M.O. acknowledges the support of EIPHI (ANR-17-EURE-0002). F.S. acknowledges the support of ERC-2020-AdG-NEUROMETA (No. 101020715). V.T. acknowledges funding from the EPSRC (EP/R01650X/1). All the Authors would like to thank the anonymous referees for the constructive suggestions that have helped to improve the quality of the manuscript.

Author contributions statement

G.C., M.O, and F.S. conceived the experiments, G.C conducted the experiments, G.C conducted the simulations, G.C., M.O, V.T., and F.S. analysed the results. All authors reviewed the manuscript.

Competing interests

The authors declare no conflicts of interest exist for the development of this work.

Data availability

The datasets used and analysed during the current study are available from the corresponding author on reasonable request.

References

1. Zhou, X. & Merzenich, M. M. Environmental noise exposure degrades normal listening processes. *Nat. Commun.* **3**, 843 (2012).
2. Basner, M. *et al.* Auditory and non-auditory effects of noise on health. *The Lancet* **383**, 1325–1332 (2014).
3. Liu, F. *et al.* On the definition of noise. *Humanit. Soc. Sci. Commun.* **9**, 1–17 (2022).
4. Tao, Y., Ren, M., Zhang, H. & Peijs, T. Recent progress in acoustic materials and noise control strategies–a review. *Appl. Mater. Today* **24**, 101141 (2021).
5. Adkins, P. Transformer noise reduction witk a close-fitting mass-law enclosure. *IEEE Transactions on Power Apparatus Syst.* **82**, 302–308 (1963).
6. May, D. The optimum weight of highway noise barriers. *J. Sound Vib.* **68**, 1–13 (1980).
7. de Melo Filho, N., Claeys, C., Deckers, E. & Desmet, W. Metamaterial foam core sandwich panel designed to attenuate the mass-spring-mass resonance sound transmission loss dip. *Mech. Syst. Signal Process.* **139**, 106624 (2020).
8. Starkey, T. A., Kyrimi, V., Ward, G. P., Sambles, J. R. & Hibbins, A. P. Experimental characterisation of the bound acoustic surface modes supported by honeycomb and hexagonal hole arrays. *Sci. Rep.* **9**, 15773 (2019).
9. D'Aguanno, G. *et al.* Broadband metamaterial for nonresonant matching of acoustic waves. *Sci. Rep.* **2**, 340 (2012).
10. Magliacano, D. *et al.* Computation of dispersion diagrams for periodic porous materials modeled as equivalent fluids. *Mech. Syst. Signal Process.* **142**, 106749 (2020).
11. Bravo, T., Maury, C. & Pinhède, C. Sound absorption and transmission through flexible micro-perforated panels backed by an air layer and a thin plate. *The J. Acoust. Soc. Am.* **131**, 3853–3863 (2012).
12. Kühl, V. & Meyer, E. Absorption of sound by porous materials. *Nature* **130**, 580–581 (1932).
13. Kuczmarski, M. A. & Johnston, J. C. Acoustic absorption in porous materials (2011). NASA report ref. NASA/TM—2011-216995.
14. Ba, A., Kovalenko, A., Aristégui, C., Mondain-Monval, O. & Brunet, T. Soft porous silicone rubbers with ultra-low sound speeds in acoustic metamaterials. *Sci. Rep.* **7**, 40106 (2017).
15. Caniato, M., Cozzarini, L., Schmid, C. & Gasparella, A. A sustainable acoustic customization of open porous materials using recycled plastics. *Sci. Rep.* **12**, 10955 (2022).
16. Jia, C. *et al.* Highly compressible and anisotropic lamellar ceramic sponges with superior thermal insulation and acoustic absorption performances. *Nat. Commun.* **11**, 3732 (2020).
17. Romero-García, V. *et al.* Perfect and broadband acoustic absorption by critically coupled sub-wavelength resonators. *Sci. Rep.* **6**, 1–8 (2016).
18. Huang, L. *et al.* Sound trapping in an open resonator. *Nat. Commun.* **12**, 4819 (2021).
19. Long, H., Cheng, Y. & Liu, X. Reconfigurable sound anomalous absorptions in transparent waveguide with modularized multi-order helmholtz resonator. *Sci. Rep.* **8**, 15678 (2018).
20. Lan, J., Li, Y., Xu, Y. & Liu, X. Manipulation of acoustic wavefront by gradient metasurface based on helmholtz resonators. *Sci. Rep.* **7**, 10587 (2017).
21. Tang, P. & Sirignano, W. Theory of a generalized helmholtz resonator. *J. Sound Vib.* **26**, 247–262 (1973).
22. Abbad, A., Atalla, N., Ouisse, M. & Doutres, O. Numerical and experimental investigations on the acoustic performances of membraned helmholtz resonators embedded in a porous matrix. *J. Sound Vib.* **459**, 114873 (2019).
23. Cummer, S. A., Christensen, J. & Alù, A. Controlling sound with acoustic metamaterials. *Nat. Rev. Mater.* **1**, 1–13 (2016).
24. Zhu, X. *et al.* Implementation of dispersion-free slow acoustic wave propagation and phase engineering with helical-structured metamaterials. *Nat. Commun.* **7**, 11731 (2016).
25. Kadic, M., Milton, G. W., van Hecke, M. & Wegener, M. 3d metamaterials. *Nat. Rev. Phys.* **1**, 198–210 (2019).
26. Assouar, B. *et al.* Acoustic metasurfaces. *Nat. Rev. Mater.* **3**, 460–472 (2018).
27. Zhao, X. *et al.* A scalable high-porosity wood for sound absorption and thermal insulation. *Nat. Sustain.* 1–10 (2023).
28. Jiang, B. *et al.* Ultralight metal foams. *Sci. Rep.* **5**, 13825 (2015).

29. Qiu, L., Liu, J. Z., Chang, S. L., Wu, Y. & Li, D. Biomimetic superelastic graphene-based cellular monoliths. *Nat. Commun.* **3**, 1241 (2012).

30. Si, Y., Yu, J., Tang, X., Ge, J. & Ding, B. Ultralight nanofibre-assembled cellular aerogels with superelasticity and multifunctionality. *Nat. Commun.* **5**, 5802 (2014).

31. Xue, H., Yang, Y. & Zhang, B. Topological acoustics. *Nat. Rev. Mater.* 1–17 (2022).

32. Yin, J. *et al.* Band transition and topological interface modes in 1d elastic phononic crystals. *Sci. Rep.* **8**, 6806 (2018).

33. Beli, D., Fabro, A. T., Ruzzene, M. & Arruda, J. R. F. Wave attenuation and trapping in 3d printed cantilever-in-mass metamaterials with spatially correlated variability. *Sci. Rep.* **9**, 5617 (2019).

34. Hu, C., Liang, B., Yang, J. & Cheng, J. Experimental demonstration of a three-dimensional omnidirectional and broadband acoustic concentrator using an anisotropic metamaterial. *Sci. China Physics, Mech. & Astron.* **64**, 244304 (2021).

35. Morandi, F., Miniaci, M., Marzani, A., Barbaresi, L. & Garai, M. Standardised acoustic characterisation of sonic crystals noise barriers: Sound insulation and reflection properties. *Appl. Acoust.* **114**, 294–306 (2016).

36. Xie, Y. *et al.* Wavefront modulation and subwavelength diffractive acoustics with an acoustic metasurface. *Nat. Commun.* **5**, 5553 (2014).

37. Singh, S. K., Prakash, O. & Bhattacharya, S. Hybrid fractal acoustic metamaterials for low-frequency sound absorber based on cross mixed micro-perforated panel mounted over the fractals structure cavity. *Sci. Rep.* **12**, 20444 (2022).

38. Gupta, A., Sharma, R., Thakur, A. & Gulia, P. Metamaterial foundation for seismic wave attenuation for low and wide frequency band. *Sci. Rep.* **13**, 2293 (2023).

39. Tang, Y. *et al.* Hybrid acoustic metamaterial as super absorber for broadband low-frequency sound. *Sci. Rep.* **7**, 1–11 (2017).

40. Xie, Y. *et al.* Acoustic imaging with metamaterial luneburg lenses. *Sci. Rep.* **8**, 16188 (2018).

41. Song, K. *et al.* Sound pressure level gain in an acoustic metamaterial cavity. *Sci. Rep.* **4**, 7421 (2014).

42. D'Alessandro, L., Ardito, R., Braghin, F. & Corigliano, A. Low frequency 3d ultra-wide vibration attenuation via elastic metamaterial. *Sci. Rep.* **9**, 8039 (2019).

43. Park, J.-H. & Lee, J.-C. Unusually high ratio of shear modulus to young's modulus in a nano-structured gyroid metamaterial. *Sci. Rep.* **7**, 1–8 (2017).

44. Jiang, Y. & Li, Y. 3d printed auxetic mechanical metamaterial with chiral cells and re-entrant cores. *Sci. Rep.* **8**, 1–11 (2018).

45. Lv, C., Krishnaraju, D., Konjevod, G., Yu, H. & Jiang, H. Origami based mechanical metamaterials. *Sci. Rep.* **4**, 5979 (2014).

46. Gatt, R. *et al.* Hierarchical auxetic mechanical metamaterials. *Sci. Rep.* **5**, 8395 (2015).

47. Zhang, Z., Scarpa, F., Bednarcyk, B. A. & Chen, Y. Harnessing fractal cuts to design robust lattice metamaterials for energy dissipation. *Addit. Manuf.* **46**, 102126 (2021).

48. Hilbert, D. & Hilbert, D. Über die stetige abbildung einer linie auf ein flächenstück. *Dritter Band: Analysis, Grundlagen der Math. Physik Verschiedenes* 1–2 (1935).

49. Thekkekara, L. V. & Gu, M. Bioinspired fractal electrodes for solar energy storages. *Sci. Rep.* **7**, 45585 (2017).

50. Maragkou, M. Fractal future. *Nat. Photonics* **8**, 817–817 (2014).

51. Fan, J. A. *et al.* Fractal design concepts for stretchable electronics. *Nat. Commun.* **5**, 3266 (2014).

52. Elwi, T. A. Printed microwave metamaterial-antenna circuitries on nickel oxide polymerized palm fiber substrates. *Sci. Rep.* **9**, 1–14 (2019).

53. Comandini, G. Sound absorption in hilbert fractal and coiled acoustic metamaterials. *Appl. Phys. Lett.* **120**, 061902 (2022).

54. Song, G. Y., Huang, B., Dong, H. Y., Cheng, Q. & Cui, T. J. Broadband focusing acoustic lens based on fractal metamaterials. *Sci. Rep.* **6**, 35929 (2016).

55. Droz, C., Robin, O., Ichchou, M. & Atalla, N. Improving sound transmission loss at ring frequency of a curved panel using tunable 3d-printed small-scale resonators. *The J. Acoust. Soc. Am.* **145**, EL72–EL78 (2019).

56. Mulholland, K. The effect of sound-absorbing materials on the sound insulation of single panels. *Appl. Acoust.* **2**, 1–7 (1969).

57. Abbad, A., Rabenorosoa, K., Ouisse, M. & Atalla, N. Adaptive helmholtz resonator based on electroactive polymers: modeling, characterization, and control. *Smart Mater. Struct.* **27**, 105029 (2018).

58. Fahy, F. J. *Foundations of engineering acoustics* (Elsevier, 2000).

59. User's, C. M. A. M. Guide, version 5.6, comsol (2020).

60. Ward, G. *et al.* Boundary-layer effects on acoustic transmission through narrow slit cavities. *Phys. review letters* **115**, 044302 (2015).

61. He, J.-H. Hilbert cube model for fractal spacetime. *Chaos, Solitons & Fractals* **42**, 2754–2759 (2009).

62. Ruiz, M. J. Hearing the transformation of conical to closed-pipe resonances. *Phys. Educ.* **52**, 035012 (2017).

63. Ayers, R. D., Eliason, L. J. & Mahgerefteh, D. The conical bore in musical acoustics. *Am. J. Phys.* **53**, 528–537 (1985).

64. Jaouen, L. & Chevillotte, F. Length correction of 2d discontinuities or perforations at large wavelengths and for linear acoustics. *Acta Acustica United With Acustica* **104**, 243–250 (2018).

65. ASTM:E2611-09. Standard test method for measurement of normal incidence sound transmission of acoustical materials based on the transfer matrix method. *ASTM Int.* (2009).

Supplementary Information

S.1 Comparison between experiments and FE models

Fig.S1 shows a comparison between experimental results and Finite Element Method (FEM) simulations for three different metamaterials configurations. The first FEM model (lossless) considers only the Helmholtz equations into account. The second FEM model (thermoviscous) accounts for the acoustic thermoviscous dissipation caused by the linearized Navier-Stokes equations. The third FEM model (narrow acoustics) takes into account the overall effects of the linearized Navier-Stokes equations, but at lower fidelity in narrow geometries. The Lossless model provides a good approximation of the experimental results in the case of the sample's holder (Fig.S1a), order zero (Fig.S1b) and the first Hilbert fractal order (Fig.S1c). However, the lossless modelling approach becomes less reliable in prediction of the TL values from the second fractal order onwards (Fig.S1d-f).

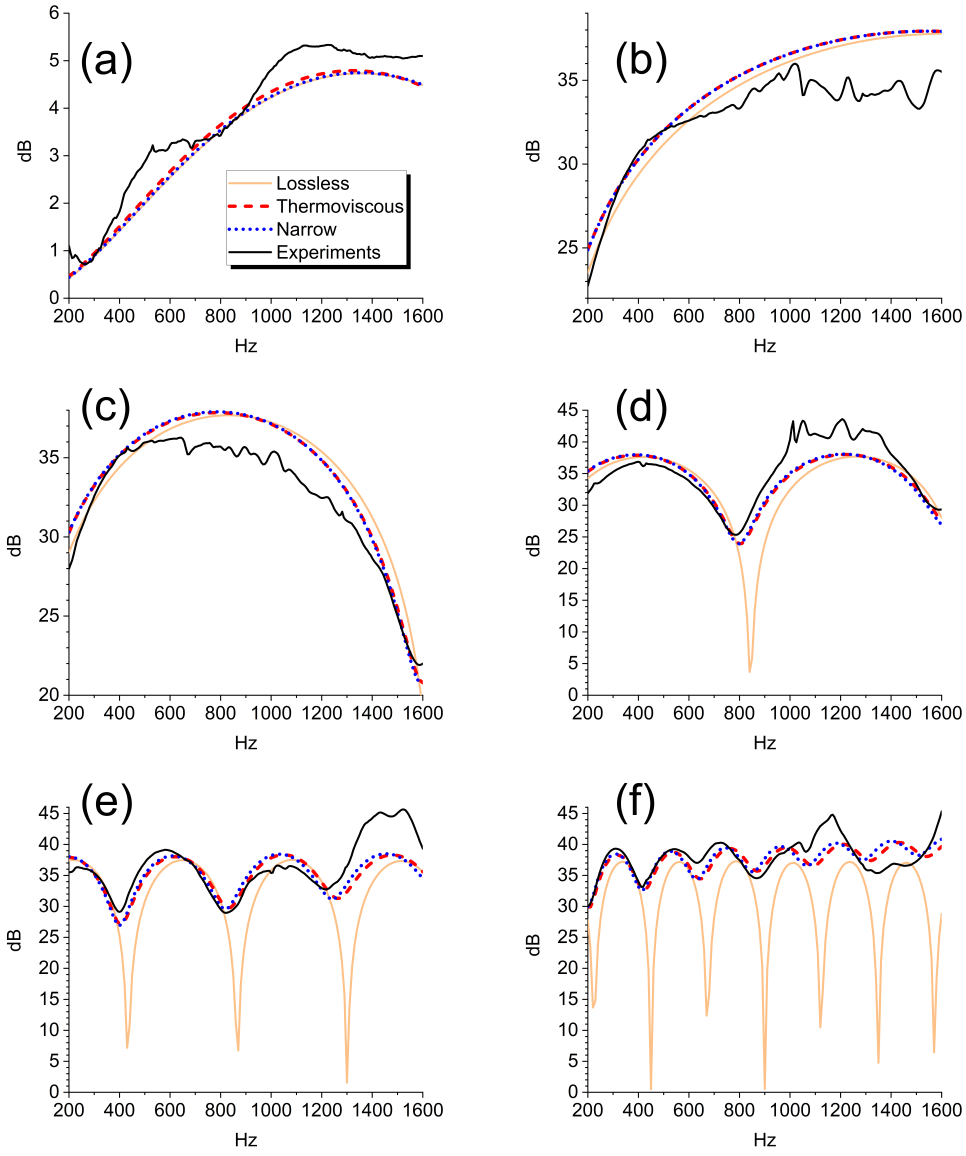

Figure S1. Comparison between results from the experiments and the three FEM models related to the holder and the Hilbert fractals. Fig.S1a, sample holder. Fig.S1b, zeroth order. Fig.S1c, first order. Fig.S1d, second order. Fig.S1e, third order. Fig.S1f, fourth order.

S.2 Comparison between the Hilbert fractal and a bulk block of PLA

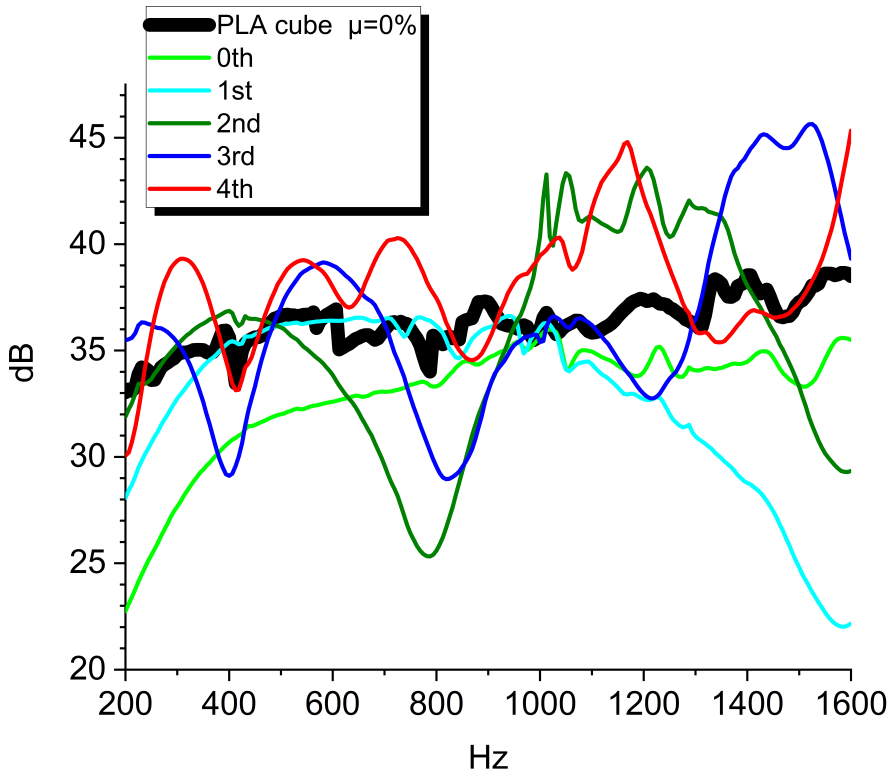

Figure S2. Values of the Transmission Loss provided by Hilbert Fractal Acoustic Metamaterials and a PLA bulk cube. The Hilbert fractal acoustic metamaterials considered here range from 0^{th} order to the 4^{th} order. The PLA bulk cube has a nominal near-zero porosity (i.e., maximum infill ratio). Notably, the transmission losses for Hilbert fractal metamaterials from the 2^{nd} to the 4^{th} order are larger than those of the PLA cube in specific frequency ranges.

S.3 Benchmark of the experimental results shown in this work against those related to other materials and FEM data

We benchmark here our experimental results against those from melamine foam[55] and polyurethane foam[56] panels with the same thickness ($50.8\,mm$), plus three different types of Helmholtz resonators. The first resonator uses an origami approach to modulate the air volume of the resonator chamber[57]. The second one uses a $3\,mm$ internal porous material[58], while the third is a classic resonator[58]. Moreover, we also show a comparison of the FEM transmission losses between the third and fourth Hilbert fractal order, and the transmission loss generated by a multi-slit array with a gap width of $0.2\,mm$, $0.5\,mm$, $1\,mm$, and $2\,mm$. The design of the slits has been taken from the work of *Ward, et al.*[60].

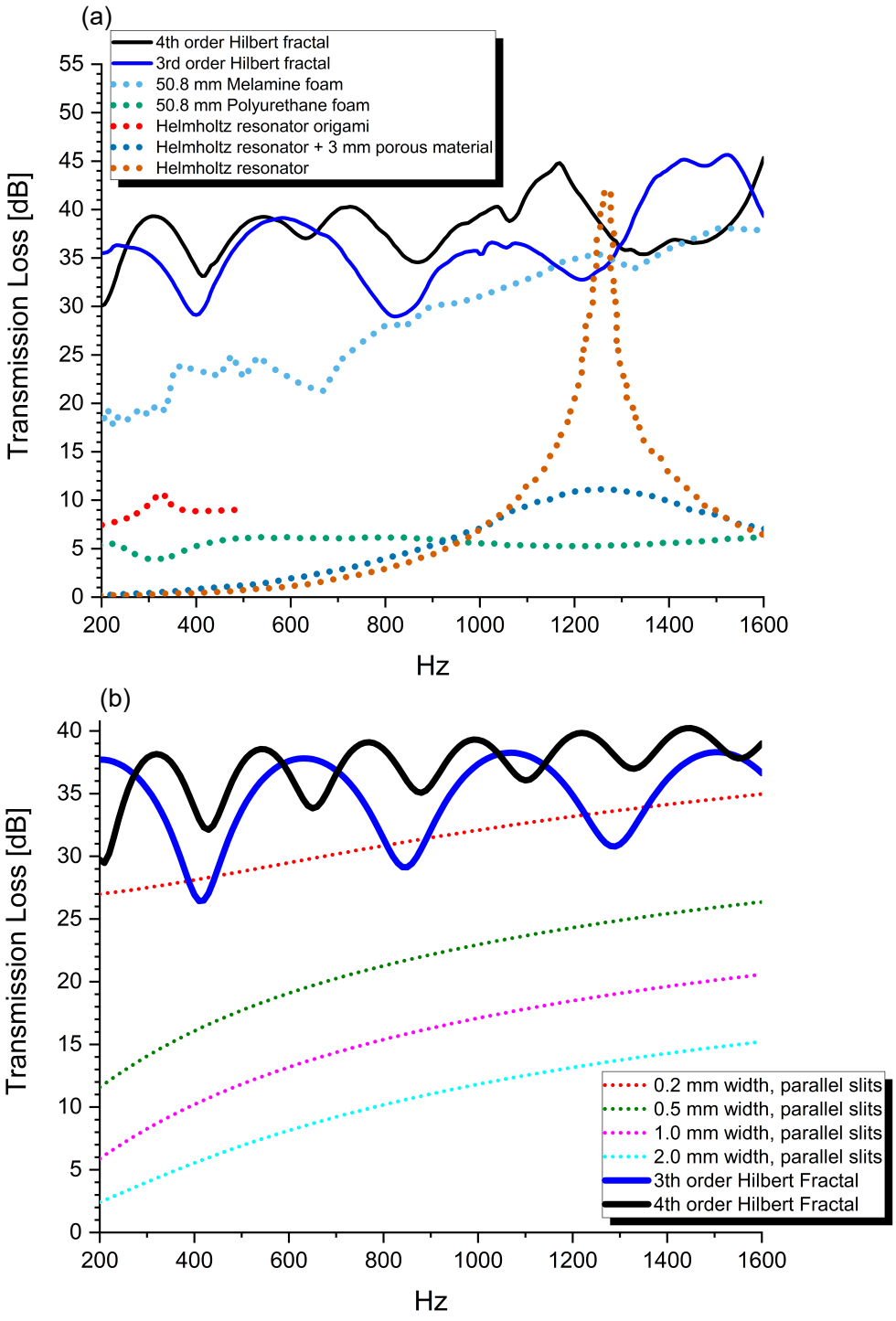

Figure S3. Figure (a) displays the experimental results for Hilbert fractal acoustic metamaterials of orders three and four, melamine foam[55], polyurethane foam[56], an origami Helmholtz resonator[57], a Helmholtz resonator with 3 *mm* of porous material[58], and a standard Helmholtz resonator[58]. All samples, including the foams and Hilbert fractals, have the same thickness of 50.8 *mm*. The Hilbert fractals demonstrate superior transmission loss behaviour in the low-frequency range, while the standard Helmholtz resonator exhibits high transmission losses in a narrowband portion of the spectra. Figure (b) shows FEM simulations related to Hilbert fractal acoustic metamaterials of orders three and four with a 1 *mm* gap width. It also includes the transmission loss related to five straight and parallel slits with gap widths of 2 *mm*, 1 *mm*, 0.5 *mm*, and 0.2 *mm*, based on the geometries described in the work of *Ward, et al.*[60].

S.4 How the fractal acoustic metamaterial generates sound transmission loss

Hilbert fractal acoustic metamaterials operate as pass filters at specific frequencies. As illustrated in Fig.S4, from *(a)* to *(d)*, when a minimum of the reflection coefficient occurs, a reduction in transmission loss happens. A single fractal geometry cavity can have multiple maxima and minima of the impedance mismatch, generating transmission loss peaks according to the overall cavity length, fractal order, side dimensions n of the cube, and gap width w.

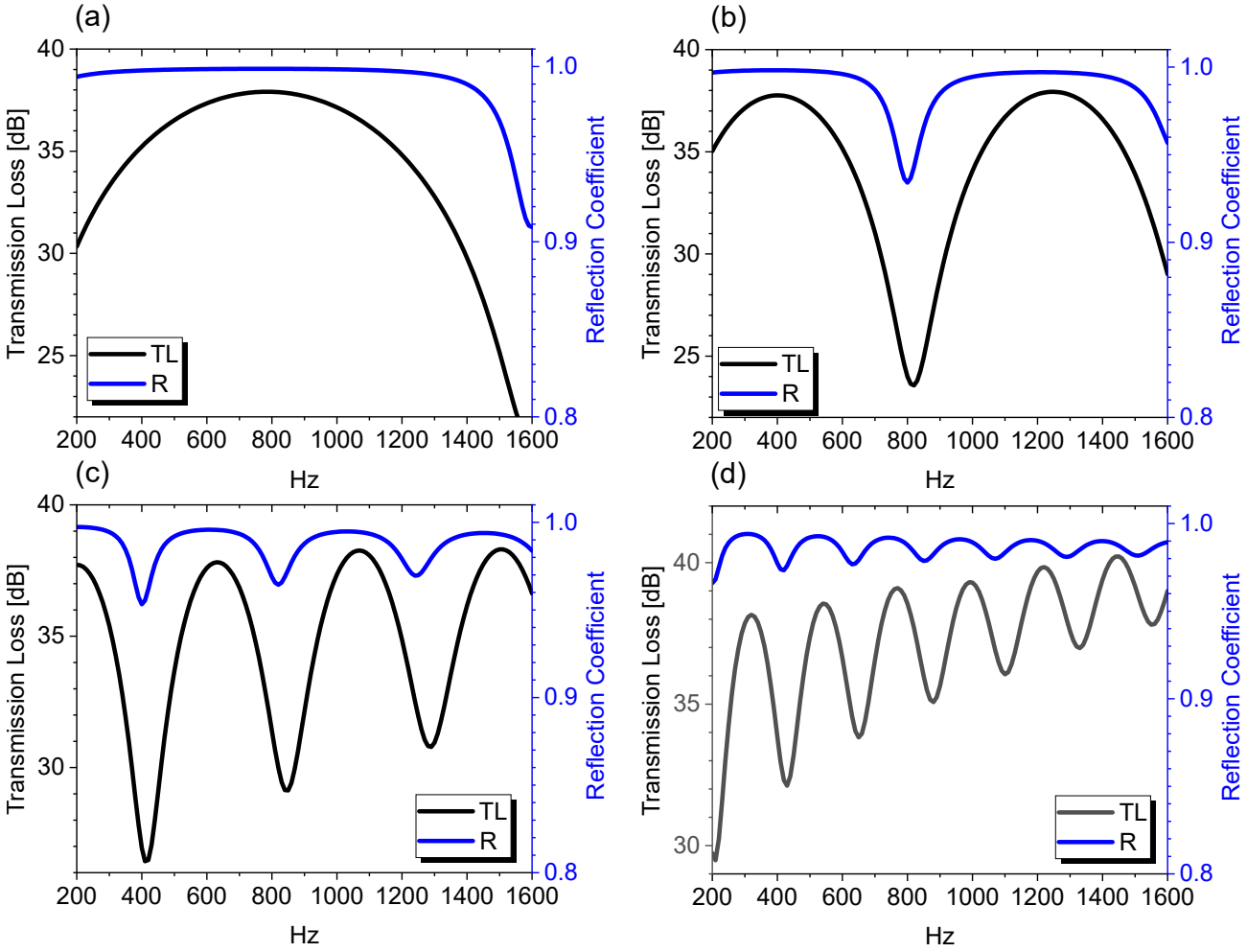

Figure S4. FEM results related to the transmission loss and reflection coefficients for $w = 1\,mm$ gap width. Subfigure (a) presents data related to the first-order Hilbert fractal, (b) for the second, (c) for the third and (d) for the fourth Hilbert fractal orders. Across all subplots, the minima of the reflection coefficient (R) correspond with drops of transmission loss (TL).

S.5 Particle velocity field

To better understand how thermoviscous air dissipation impacts the propagation of acoustic waves within narrow channels, we show the particle velocity field in the lower section of the fractal pattern where the inlet and outlet are positioned (Fig.S5) This plots demonstrate a distinct contrast between the finite element model accounting for the thermoviscous dissipations and the lossless model. This difference becomes particularly apparent as the fractal order increases, and hence the channel length becomes larger. The data clearly show significant discrepancy between predicted and experimented transmission loss occurs when ignoring the effect of the thermoviscous dissipation, as underlined by *Ward, et al.*

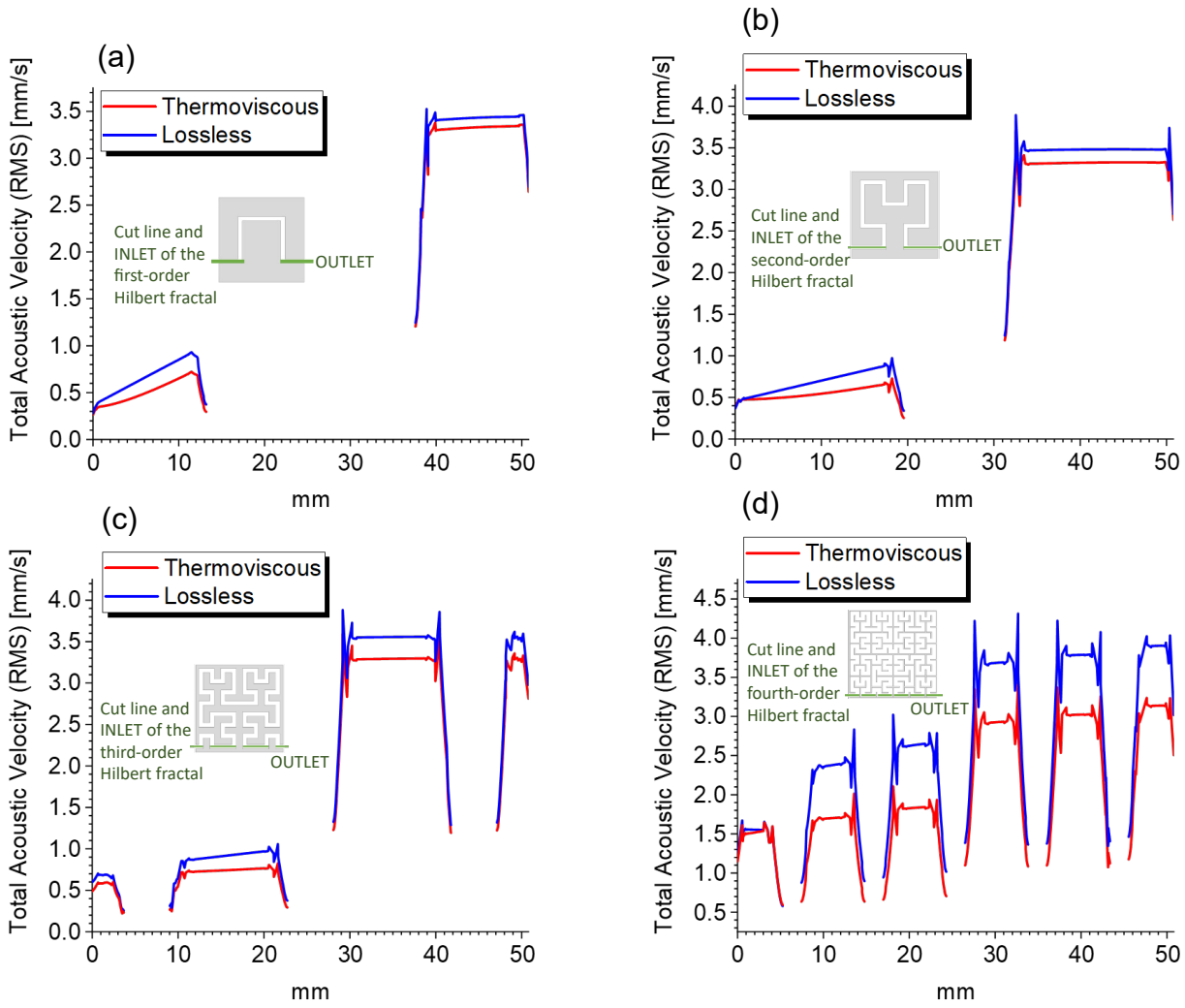

Figure S5. The four subfigures (a, b, c, d) show the total root mean square acoustic velocity in mm/s along a representative line passing through the middle of the inlet and outlet of metamaterials with $w = 1\,mm$ and $n = 50.8\,mm$. Each subfigure presents two FEM simulations: one assuming lossless behavior within the small fractal pattern channels, and the other with a thermoviscous air model. Subfigure (a) illustrates the section line of the first-order Hilbert fractal, represented by a green segment. The absence of a velocity representation in parts of the graph corresponds to the solid portions of the fractal, where air is not present. This pattern is mirrored in subfigures (b), (c), and (d), which are related to the second, third, and fourth-order Hilbert fractals, respectively.

S.6 Normalised standard deviation

Normalised standard deviation for the three different ΔL considered in Eq.1 for every acoustic mode within the frequency range investigated. In the case of $\Delta L = 0$, we observe a fast degeneration of the frequency predicted for acoustic modes after the first. $\Delta L = \frac{8w}{3\pi}$ is the best predictor for the frequencies corresponding to the TL maxima within the gap width range considered in this work. A possible correction for the channel length is $\Delta L = \frac{8}{3\pi^{\frac{3}{2}}}\sqrt{nw}$[60]; when using this expression, one can observe a slightly worse prediction that the one provided by $\Delta L = \frac{8w}{3\pi}$. This is true for all the fractal orders of the metamaterials, apart from the 0^{th} one, for which we have a simple slit without any ninety-degree angles inside. The calculation to normalise the standard deviation is the following:

$$NSD = \frac{A - B}{C} \tag{2}$$

Where NSD is the normalised standard deviation along the several gap widths analysed. A is the average value of the acoustic mode with Eq.1. B and C are the average FEM values for the acoustic modes and for the standard deviation.

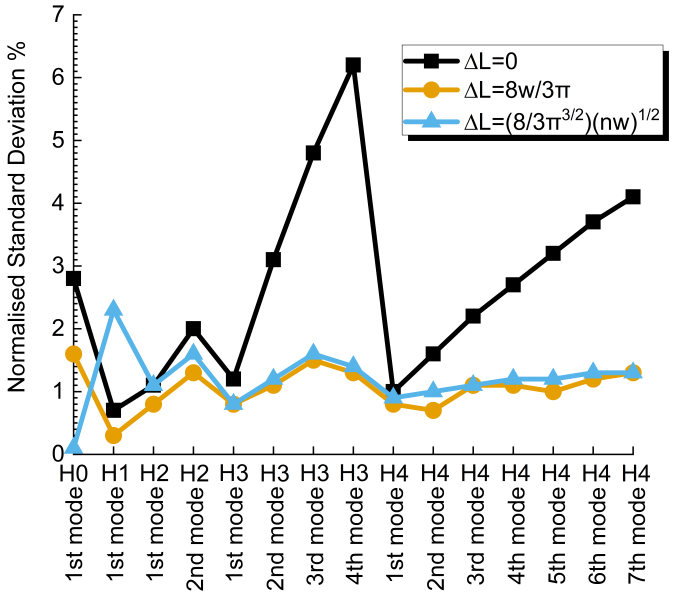

Figure S6. Comparative analysis of the three analytical formulas predicting the frequency position of transmission loss peak between $200\,Hz$ and $1600\,Hz$. The normalised standard deviation is calculated as the difference between the average value of the acoustic modes from the analytical formulas and the FEM simulations, divided by the standard deviation of the frequencies from the FEM simulations. The three formulas differ in considering the correction of the channel length within the fractal. The first formula does not account for any artificial length correction and maintains a reasonably low normalised standard deviation only for the first acoustic mode of the fractals, with an increasing deviation for subsequent modes. The second formula, which considers an artificial elongation as a function of the gap width (w), maintains a low normalised standard deviation across all investigated acoustic modes. The third formula, which considers a length correction as a function of the fractal slit area, also maintains a low normalised standard deviation across all modes but performs worse than the second formula, except for the first acoustic mode of a simple slit without fractal geometry.